Electronic Supplementary Material (ESI) for Nanoscale.

Supplementry Information

Monitoring Interfacial Lectin Binding with Nanomolar Sensitivity Using a Plasmon Field Effect Transistor

Hossein Shokri Kojori[a], *Yiwen Ji*[b], *Younghun Paik*[a], *Adam B. Braunschweig*[b,c,d,*], *and Sung Jin Kim*[a,e,*]

[a]Department of Electrical and Computer Engineering, University of Miami, FL

[b]Department of Chemistry, University of Miami, FL

[c]Advanced Science Research Center (ASRC), City University of New York, New York, New York 10031, United States

[d]Department of Chemistry and Biochemistry, City University of New York—Hunter College, 695 Park Avenue, New York, New York 10065, United States

[e]Biomedical Nanotechnology Institute at the University of Miami (BioNIUM), FL

Table of Contents

1. Plasmon Field Effect Transistor Fabrication

The plasmon field effect transistor was made following previously reported literature protocols[1]. The fabricated FET devices were characterized regarding their electrical performance before gold NPs were incorporated onto the active layers. The dimensions of the fabricated devices was 100 µm and 50 µm of channel length (L) and width (W), respectively. Also the open area onto which the Au NPs were assembled was 30 µm × 100 µm. The images of the device structure using an optical microscope a scanning electron microscope (SEM) and I-V characteristic of fabricated field effect transistor under dark and light conditions are shown in Figure S1.

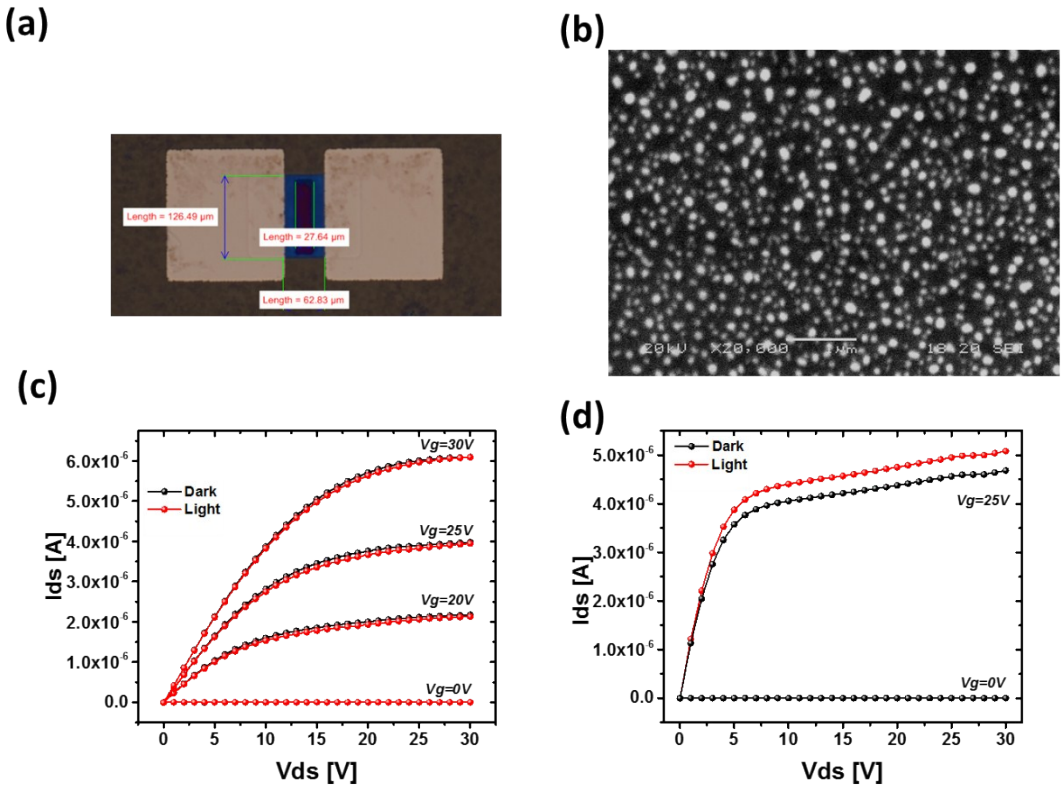

Figure S1. a) Micrograph of fabricated plasmon FET. b) SEM picture of Au NPs (JEOL JSM 5601 LV SEM). Scale bar is 1 µm and c) *I-V* characteristic of fabricated FET c) without and d) with Au NPs under dark and light illumination.

2. Binding studies.

Operating principles of the plasmon FET. The operating principles of the plasmon FET were reported previously[1], and are summarized below. In the plasmon FET, the plasmonic absorption of Au NPs generates hot electrons, and these high energy hot electrons can overcome the Schottky barrier and diffuse to the IGZO film (Fig.1a). Consequently, this process provides more electrons in the IGZO channel which results in increased channel conductivity and drain current (I_d). Because the number of hot electrons than can overcome Schottky barrier depends on the plasmonic absorption of gold NPs, the resulting drain current response as a function of wavelength should be matched with the absorption spectrum of Au NPs. The induced Plasmonic hot electrons are accumulated at the n-channel that was created by the gate voltage bias. Therefore, the plasmonic hot electrons in channel will increase the drain current by the factor that is based on the drain current equation of FET saturation mode. Therefore, the plasmon-FET converts localized surface plasmon energy to flowing electrical charges. Plasmon energy was further amplified with gate voltage bias, by increasing the quantum tunneling efficiency of electrons from the Au NPs into the IGZO channel.

Applying positive gate voltage to the plasmon-FET results in electron accumulation in the n-channel inside the IGZO and close to the SiO_2 layer. The spatial difference of electron density generates a large potential gradient from the floating ground (Au NPs) to the area of induced plasmonic hot electrons accumulation. This internal electric field created by the gate bias enhances electrons movement to the other boundary where the FET channel is located. The induced plasmonic hot electrons are seized by the gate voltage, consequently contributing to channel enhancement and generating more drain current to flow. As a result, the collected drain

current is proportional to the plasmonic absorption from the Au NPs. However, it is not saturated due to the limited number of hot electrons generated in the Au NPs.

3. Absorption spectrum of Au NPs

To fabricate the Au NPs, 5 nm of Au thin film was deposited on top of a glass substrate with an electron-beam evaporator. The Au NPs were formed by a thermal reflow process[4] as described earlier. Figure S2 shows the absorption spectrum of Au NPs, with an absorption maximum at 550 nm. The absorption spectrum was measured using conventional spectrometer setup with a white light source (Quartz Tungsten Halogen lamp (250W), Oriel) and a spectrometer (StellarNet, BLACK-Comet Concave Grating).

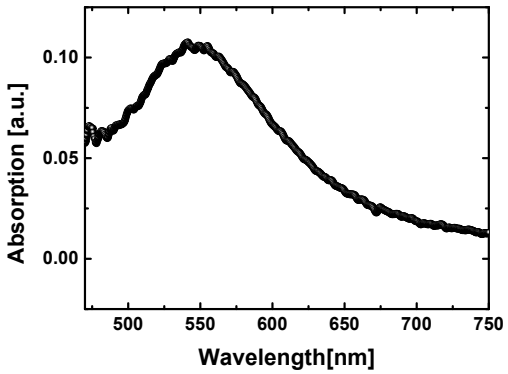

Figure S2. Absorption spectrum of Au NPs on top of the glass substrate

4. The sensing platform electrical circuit

Figure S3 shows the cicuit which was used to measure the sensors. D, G and S represents drain, Gate and source. The sensors are biased in saturation mode and the measurements was done by Lock-in amplifier.

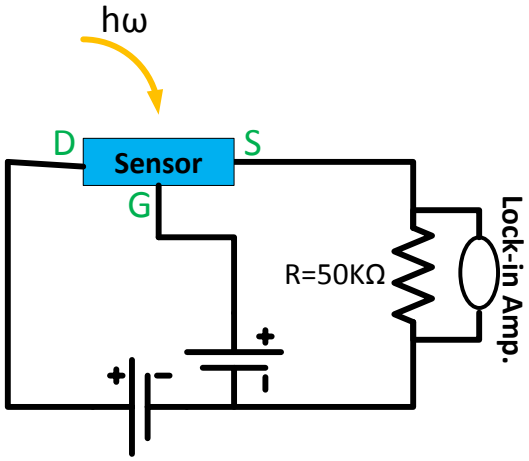

Figure S3. Electrical circuit to measure the plasmon FET based sensors.

5. Plasmon FET response at different wavelengths

Figure S4 shows the plasmon FET sensor responses at different excitation wavelengths (480 nm − 700 nm). To measure this data the same circuit shown in Figure S3 was used. As it can be seen in this figure the plasmon FET has higher response at 500 nm, which means that the Plasmon FET generates more hot electrons at 500 nm than 600 nm, and as a result the response of the sensor follows the absorption spectrum of Au NPs as shown in Figure S2.

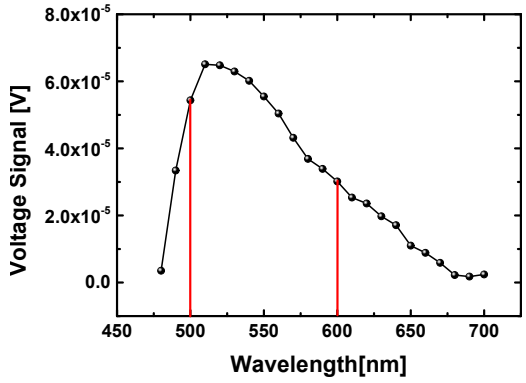

Figure S4. The reference sensor generated signal at each wavelength

6. LSPR based sensor measurements (control experiment)

To measure the ConA-glycopolymer binding in a conventional LSPR architecture, where the change in absorption spectrum is used to indicate binding, the same Au NP-glycopolymer conjugates were patterned on top of a glass substrate. Using a white light source (Quartz Tungsten Halogen lamp (250W), Oriel) and an optical spectrometer (StellarNet, BLACK-Comet Concave Grating), the absorption spectrum of Au NPs was obtained while the sensors were exposed to different concentrations of ConA (2.1×10^{-9} M − 2.1×10^{-6} M). Figure S5 shows the experiment diagram for LSPR based sensor measurement. White light was brought to the LSPR sensor from a halogen lamp using an optical fiber and two objective lenses to collimate and focus the light onto the sample. Using another optical fiber, the transmitted light was brought to the spectrometer, and the absorption spectrum was calculated.

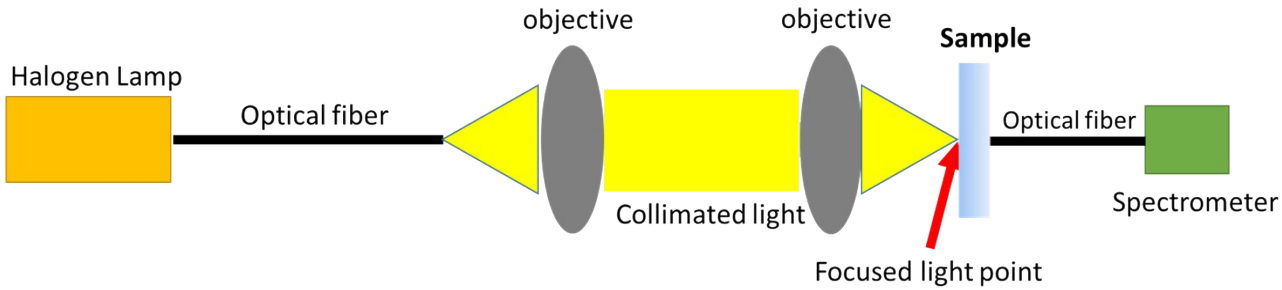

Figure S5. LSPR based sensor measurement diagram. Two objective lenses were used to collimate the light and focus on top of the sample. The fiber optic tip behind the sample gathered the transmitted light through sample and brought light into the spectrometer.

7. Measured sensor response for control proteins

The plasmon FET was exposed to PSA, PNA, and GNA following an identical procedure to that used for the ConA. Figure S6 a,b shows the sensor response for PSA and GNA, and PNA respectively. For GNA and PNA no significant sensor response was observed at a protein concentration of 2.1E-5 M, which was the concentration that the sensor saturated for ConA. The reference signal (black line) in Figure S6 are the signal from the plasmon FET sensors before introducing the target proteins to the sensor surface. The reference sensor has glycan and BSA.

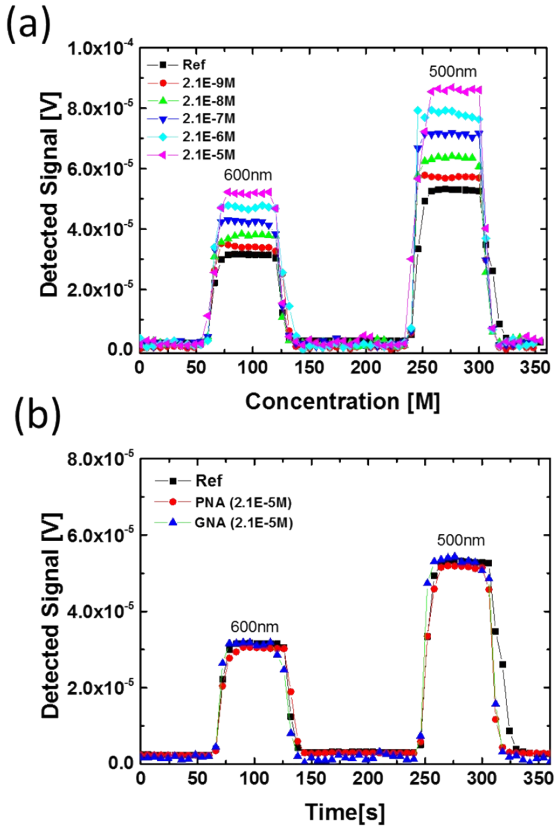

Figure S6. The measured sensor response under 500 nm and 600 nm with a) PSA and b) GNA and PNA proteins.

8. Statistical analysis of plasmon FET

To study the device-to-device variation, plasmon FET sensors were functionalized with glycopolymer, and four of each sensor were exposed to different concentration solutions of ConA. All the sensors were measured using same techniques described in the main text. Figure S7 shows the measured data of the sets of four different sensors exposed to two different concentrations of ConA (1.0×10^{-6} and 2.1×10^{-6} M). The statistical analysis (average and standard deviation) over the four devices in each set is shown in Figure S8 which confirms that the proposed sensing platform has a maximum standard deviation of 4.3% at 600 nm. The plasmon FETs that were used for statistical analysis has a slightly different electrical scheme than the ones in the main manuscript as a result of changes to the device fabrication protocol.

Specifically, the new devices had higher drain current under the same voltage bias condition than the devices in the manuscript (Figure 3). However, the experimental results indicate negligible device-to-device variation regardless of the fabrication process (Figure S9). Moreover, the calculated K_a values for these sensors are very similar to the sensors in the manuscript (1.28×10^7 M^{-1} in manuscript and 1.15×10^7 M^{-1} for the high drain current sensors), which confirms that our sensing system is robust. In addition, by calculating the normalized generated signal by these high drain voltage sensors and superimposing this data onto the data from Figure 3 of the manuscript we can see that regardless of the electronic scheme, the data is in good agreement. This data is presented in figure S9.

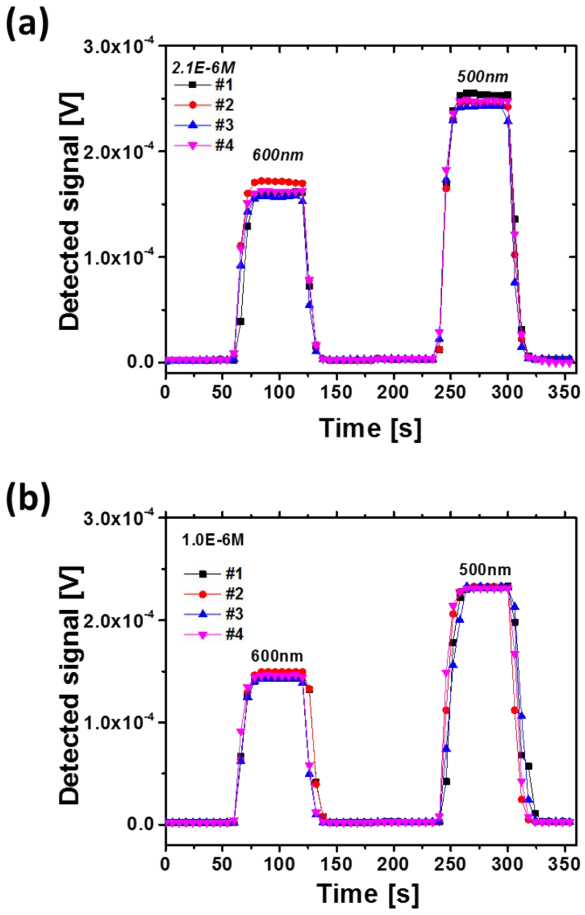

Figure S7. The measured four sensors responses to the same ConA concentration are superimposed at a) 2.1×10^{-6} M and b) 1.0×10^{-6} M.

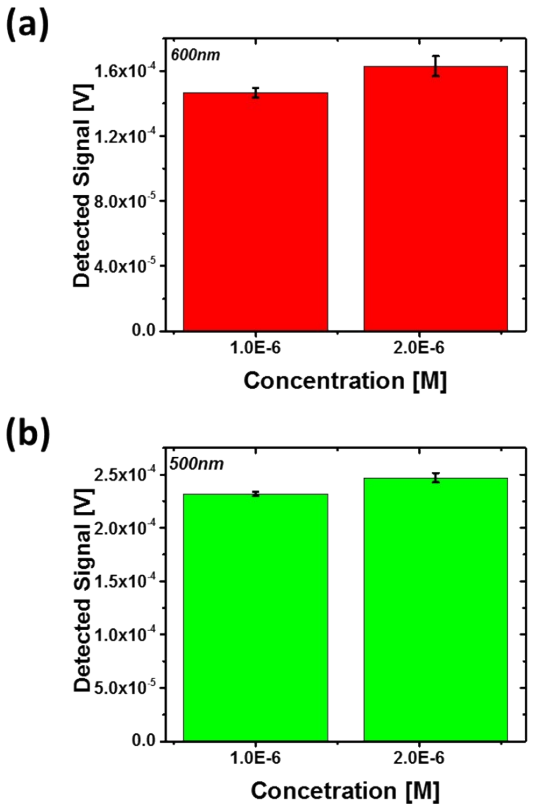

Figure S8. Average and standard deviation of detected signals from the plasmon FETs at a) 600 nm and b) 500 nm.

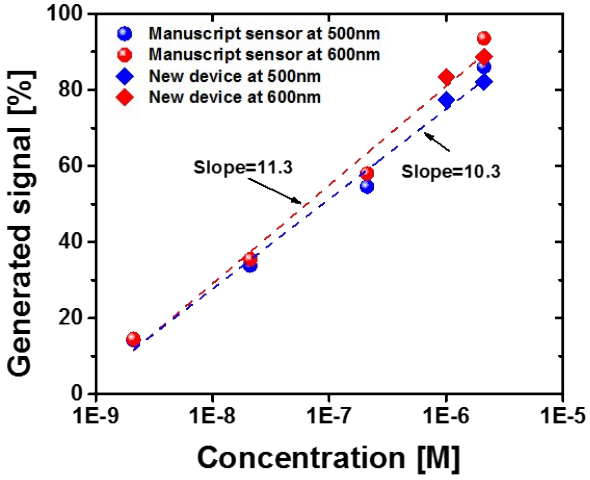

Figure S9. Normalized generated signal of new sensors fitted into the data from the sensors in manuscript. The new sensor data is the average values from 4 different devices at each concentration. The standard deviation of the measured data from the new devices are 2% and 4.3% for 500 nm and 600 nm optical illumination, respectively.

9. The sensor response without Au NPs

To demonstrate that the plasmon FET only detects signal due to the interaction of lectin-glycan on topf Au NPs, a sensor was fabricated without Au NPs. Then, the same protocol was used to expose the sensor to a 2.1×10^{-6} M solution of ConA. Figure S10 shows the measured signal at two wavelengths (500 and 600 nm). There is no detected signal when Au NPs are not on top of the FET structure because Au NPs are the source of plasmonically-induced hot electrons under illumination of light.

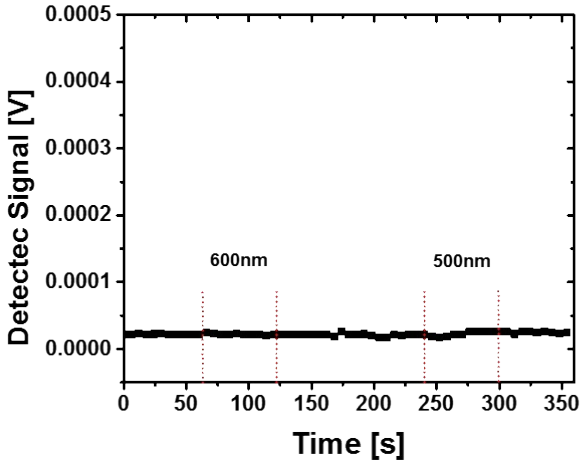

Figure S10. The measured sensor response under 500 nm and 600 nm without Au NPs

10. The sensor response with different hosting buffer

To study the effect of buffer change on sensor response, two sensors were tested with the same concentration of ConA (1×10^{-6} M) in Tris-Buffered Saline (TBS) and PBS buffers. Figure S11 shows sensors responses in PBS and TBS where the sensor in TBS shows lower detected signal. The association constant (K_a) for the sensor with PBS is $1.15 \pm 0.12 \times 10^7$ M^{-1} and for the sensor in TBS is $0.82 \pm 0.08 \times 10^7$ M^{-1} at 600 nm

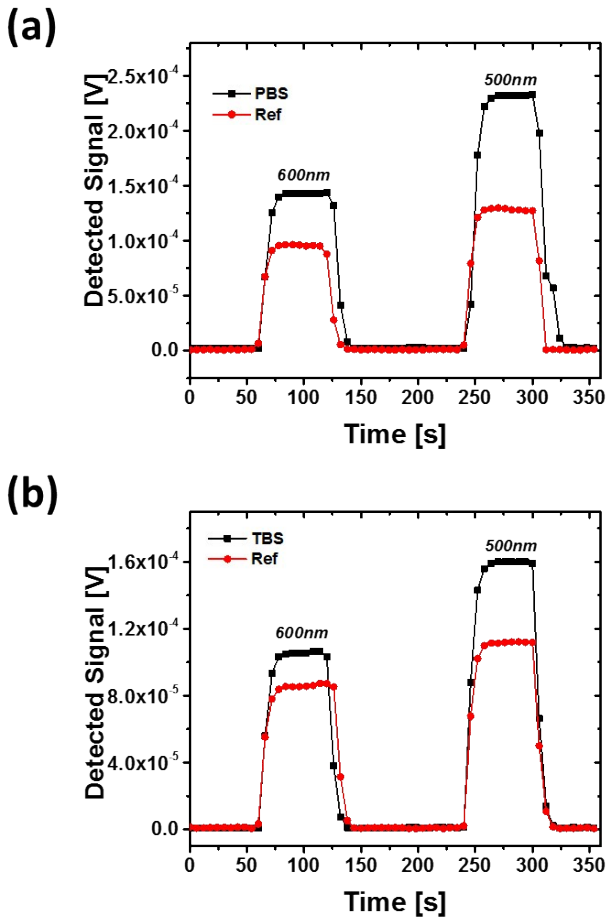

Figure S11. The measured sensor response in a) PBS and b) TBS buffer with the same concentration of ConA (1.0×10^{-6} M).

11. Statistical analysis on LSPR-based sensors

Three different glass substrates with patterned Au NPs were prepared. These samples went through the same glycopolymer functionalization as the plasmon FETs, and exposed to different concentrations of ConA, as described in the main text, and the absorption spectra were measured by using the method described in section 6. Statistical analysis are presented in figure S12 which shows the LSPR based sensor has a standard deviation of 10%.

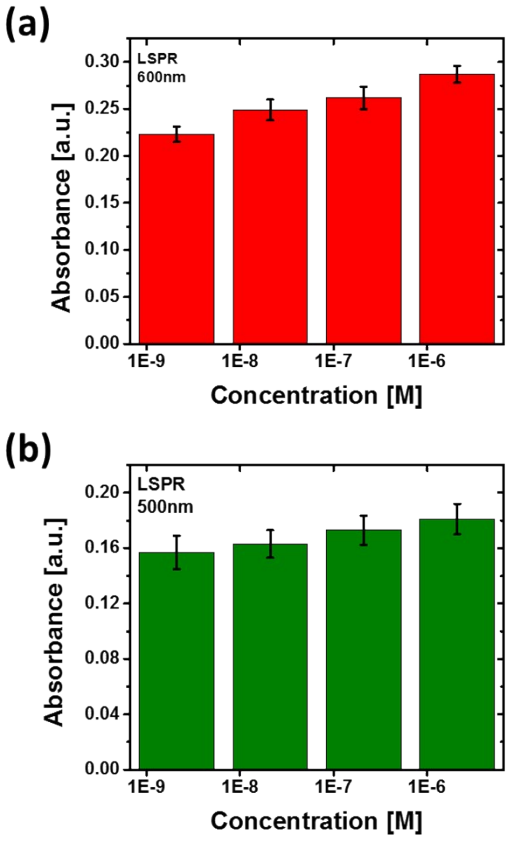

Figure S12. The average and standard deviation of LSPR based sensors upon exposure of ConA solutions (2.1×10^{-6}, 2.1×10^{-7}, 2.1×10^{-8}, and 2.1×10^{-9} M) at (a) 600 nm and (b) 500 nm illuminations.

12. Ka value calculation and plots

We used the Langmuir adsorption isotherm: $\frac{\Delta R}{\Delta R_{max}} = \frac{K_a[P]}{1+K_a[P]}$ to calculate the K_a values. And the details are well described in ref 49-51. Ka is calculated by finding the minimum value of the sum of $(\theta - \theta')^2$, where $\theta = \frac{\Delta R}{\Delta R_{max}}$, and $\theta' = \frac{K_a[P]}{1+K_a[P]}$. Following two plots show Normalized LSPR shift, ΔR/ΔRmax versus binding response curve for the specific binding of lectins to glycopolymer functionalized gold NP surface.

The solid line is the calculated value of $\Delta R/\Delta R_{max}$ using the Langmuir adsorption isotherm equation with a calculated Ka value.

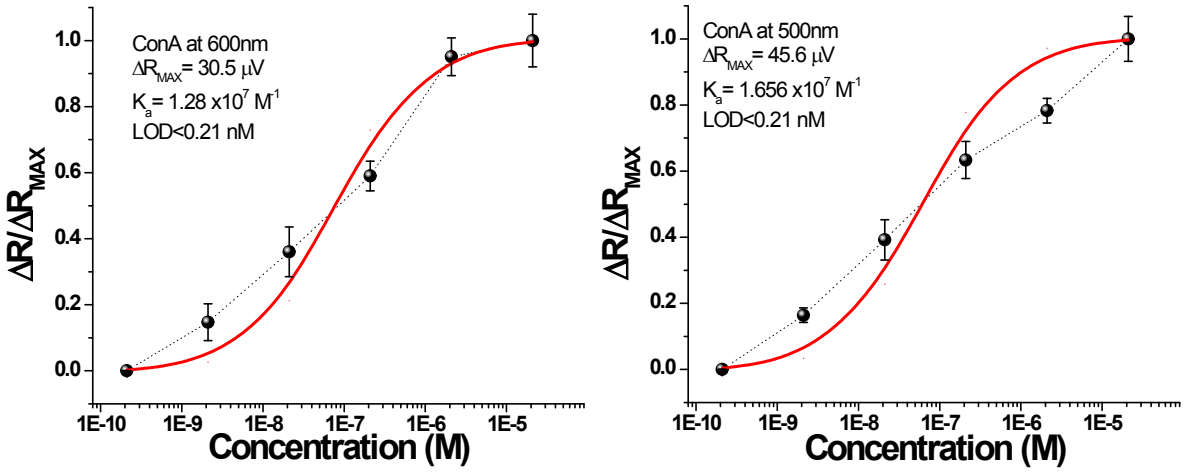

(a) (b)

Figure S13. Normalized plasmon FET response (solid dots), $\Delta R/\Delta R_{max}$ versus binding response curve (solid line) under (a) 600nm illumination and (b) 500nm illumination. The solid line is plotted using the calculated values of K_a (1.28×10^7 M^{-1} and 1.656×10^7 M^{-1} for 600 nm and 500 nm responses, respectively) using the Langmuir adsorption isotherm equation . In both cases, the limit of detections are 0.21 nM. The error bars are from multiple measured values.

References.

1. H. Shokri Kojori, J.-H. Yun, Y. Paik, J. Kim, W. Anderson, S. J. Kim, *Nano Lett.* **2016**, *16*, 1.
2. Y. K. Lee, C. H. Jung, J. Park, H. Seo, G. A. Somorjai, J. Y. Park, Y. *Nano Lett.* **2011**, *11*, 10.